International Journal of Design & Nature and Ecodynamics
Vol. 21, No. 3, March, 2026, pp. 671-683
Journal homepage: http://iieta.org/journals/ijdne

Preparation of Ca/Al-LDH Alginate Beads from Industrial By-Products for Amoxicillin Removal in Groundwater Remediation

Anfal E. Khalaf*, Ayad A. H. Faisal

Department of Environmental Engineering, College of Engineering, University of Baghdad, Baghdad 10011, Iraq

Corresponding Author Email: anfal.enad2311@coeng.uobaghdad.edu.iq

https://doi.org/10.18280/ijdne.210306

Received: 29 December 2025
Revised: 15 February 2026
Accepted: 23 February 2026
Available online: 31 March 2026

Keywords:
sorbent, alginate beads, amoxicillin, permeable reactive barrier, waterworks sludge treatment, cement kiln dust, layered double hydroxides

ABSTRACT

This study reports the synthesis of a novel, low-cost sorbent prepared from readily available industrial byproducts, namely Ca/Al LDH nanoparticles immobilized in sodium alginate beads (Ca/Al nanoparticles@Na-alginate beads). The sorbent was designed for continuous treatment of amoxicillin (AMX)-contaminated groundwater using a permeable reactive barrier (PRB). The beads were manufactured from byproducts, mainly waterworks treatment sludge (WTS), which resulted in huge quantities from the activities of the water supply treatment system, and cement kiln dust (CKD) resulting from the production of cement, to fulfill the sustainability requirements. The sorbent was made by creating nanoparticles from layered double hydroxides (LDHs) of calcium and aluminum, which were subsequently immobilized using sodium alginate. The precipitation process was used to create these particles. The molar ratio (Ca/Al) = 1:1, solution pH = 10, and Ca to Al nanoparticle dose = 5 g per 100 mL are the ideal conditions for bead preparation to achieve maximal AMX removal efficiency. Material characterization confirmed successful incorporation of the nanoparticles into the beads, which enhanced antibiotic sorption. PRB performance was positively correlated with bed thickness (60 cm) and negatively correlated with flow rate (2 mL/min) and influent AMX concentration (10 mg/L). The Bohart–Adams, Thomas–BDST, Yan, Belter–Cussler–Hu, and Clark models were fitted to the experimental breakthrough data for AMX removal.

1. INTRODUCTION

One of the most common sources of water is groundwater, which is more reliable for a variety of applications than surface water [1, 2]. Because the majority of pollutants emitted from anthropogenic and/or natural activities are harmful and have both acute and long-term toxicity effects, the pollution of this resource is a serious environmental problem [3-8]. The United States Environmental Protection Agency (EPA) figures show that the cleaning of over 217,000 contaminated sites cost 190 billion dollars [9].

The idea behind the technology of pump-and-treat (P&T) is to extract contaminated groundwater so that it can be remediated at the ground surface by traditional techniques. The resulting water may be dumped into a sewer system, injected into the subsurface, or released into a surface water stream. For a number of years, this method has been extensively employed at numerous contaminated locations. Unfortunately, there is evidence that this approach is frequently inappropriate for ongoing cleanup of contaminated areas. Although the pump-and-treat approach was successful in the early stages, data gathered from these sites showed that its efficacy was significantly low in the long run [10, 11]. As a result, researchers developed the permeable reactive barrier (PRB) as a substitute way to address the flaws and limitations of the P&T approach. The PRB must be positioned perpendicular to the contamination plume routes and consists of a trench filled with the proper reactive material. The contamination molecules are either sorbed or decomposed when polluted water seeps through the wall. In order to ensure that the entire contamination plume is intercepted and to provide sufficient residence time for efficient remediation, the wall design must be carefully examined for its proportions. A suitable reactive medium must also be carefully chosen in the interim [12]. Activated carbon [13], zeolite [14], and zero-valent iron are just a few examples of the various materials that can be found in PRBs for both organic and inorganic contaminants [15]. Olive pips [16], cement kiln dust (CKD) [17], waterworks treatment sludge (WTS) [18], waste foundry sand [19, 20], sewage sludge [21, 22], zero-valent iron/aluminum [23, 24], iron slag [25, 26], and other sorbents [5, 27-30] were among the industrial byproducts that were used as reactive materials in many prior studies. The new approach taken in recent investigations was the synthesis of novel sorbents from byproduct wastes. Humic acid, for instance, is collected from the sludge of sewage and accommodated on the surfaces of sand [31]. Hydroxyapatite (HAP) is made from leftover eggshells because of its high calcium content, affordability, and accessibility [32, 33]. The chemical structure of calcium hydroxyapatite (Ca-HAP), which has a compatible nature, is $Ca_{10}(PO_4)_6(OH)_2$ [34]. It is a biologically friendly inorganic substance [34].

Due to widespread use and incomplete removal, pharmaceuticals have emerged as contaminants of emerging concern in aquatic environments. Many pharmaceuticals, including antibiotics, chemotherapeutic agents, antipyretics, contraceptives, antidepressants, medications, and analgesics, are likely released into aquatic systems during production and usage without any adequate remediation [35]. Among these medications, antibiotics are widely used as veterinary, clinical, and animal growth-promoting medications. The frequent use of various antibiotics has resulted in a huge increase in pathogens that are resistant to common antibiotics, which is a serious threat to human health as well as other organisms [36, 37]. This is one of the main concerns regarding rising rates of antibiotic tolerance to various kinds of bacteria. A common medication for animals, amoxicillin (AMX), can be discharged and build up in natural water resources, posing a major risk to the aquatic environment and human health. The removal methods used to successfully remove AMX technologies were examined [38, 39]. The most common techniques for getting rid of pharmaceutical effluent are chemical and biological procedures. When it comes to removing AMX from wastewater, advanced oxidation, electrochemical degradation, and electrocoagulation techniques are all reasonably successful [40, 41].

The nature of the changes that occur on the surface of the (Ca/Al)-LDH-alginate beads due to interaction with AMX antibiotic plays a major role in the adsorption mechanisms in the prepared adsorbent. Aluminum and calcium ions dominate the adsorption properties, as it is characterized by the presence of positive surface charges in addition to internal anionic charges [42]. The study confirmed that the removal is most efficient at pH 3, then the formation of zwitterion will occur, carrying both positive charge by the amine and negative charge by the carboxyl. At this pH, the LDH will carry a positive charge on its surface. As a result, the process will include two mechanisms: the first is the chemical bonding of carboxyl groups with the positively charged surface, associated with aluminum and calcium ions. The second mechanism includes the ion exchange of negative charges with the anions in the LDH structure. Furthermore, the hydrogen bonding and adsorption on the surface are minor suggested mechanisms [43]. Based on the fact that adsorption follows the pseudo-second-order, the first mechanism is the governing mechanism.

Previous research indicated that the ambiguity in the practical sector cannot be explained by the cost, effectiveness, and stability of the specified approaches. On the other hand, adsorption emerged as a method that is simple to implement, inexpensive, adaptable, and capable of treating a variety of contaminants; hence, this approach may be more appropriate for handling such a situation [41]. Water contaminated with organic contaminants can be cleaned up using a variety of adsorbents, including fly ash, sawdust, clay, activated carbon, polymers, and materials coated with nanoparticles [37, 44, 45]. Lately, research has focused on producing LDHs for use in the realms of electrochemistry, magnetization, and the environment. The relationship between metal ions in the presence of anions is the foundation of LDHs.

The current study's objectives are to: i) determine whether waterworks sludge (as Al source) and CKD (as Ca source) may be used as low-cost sorbents in PRBs to remove AMX from contaminated groundwater; and ii) identify the governing mechanisms in charge of the removal process.

2. METHODOLOGY OF LABORATORY WORK

2.1 Instrumentation

X-ray Diffraction (XRD) pattern was recorded on a Shimadzu-7000, Japan, in the range 2θ = 5-80°. Scanning Electron Microscopy (SEM) images were acquired using an Oxford model, using the gold coating method for the preparation of the sample. Transmission Electron Microscopy (TEM) images were obtained using a JEOL TEM. A drop of the nanoparticle suspension was deposited onto a carbon-coated Cu grid and dried at room temperature.

UV-Vis was used to monitor the AMX concentration after each experiment using a device with a model of Shimadzu 1800, Japan, at a wavelength of 227 nm.

The "state company for the Drugs Industry and Medical Appliances" in Samarra, Iraq, provided AMX. It was chosen to mimic the pharmaceutical organic contaminant contaminating groundwater. To achieve the necessary concentrations, a 1000 mg/L aqueous solution of AMX ($C_{16}H_{19}N_3O_5S$) was produced and diluted. The solution pH was changed with sodium hydroxide or 0.1 M hydrochloric acid.

In order to manufacture (Ca/Al)-LDH nanoparticles, CKD was collected at the Kirkuk Cement Factory in Iraq. By "Le Chatelier flask and ASTM C188–95 (Standard Test Method for Testing Density of Hydraulic Cement)", CKD specific gravity was found to be 2.77. Due to the wide variety of particle sizes found in its particle size distribution curve, this dust is categorized as a heterogeneous substance [46].

The waterworks sludge used in the current studies came from the AL-Weihdaa water treatment plant in Baghdad, Iraq. To clean the raw water, alum salts are constantly supplied to the sedimentation tank. The sludge was crushed, allowed to air dry for several days, and then ground into a powder.

2.2 Manufacturing of sorbent

LDHs were prepared via a co-precipitation route conducted at room temperature. Calcium and aluminum ions were obtained by acid extraction as follows:

Step one: 140 mL 25% (v/v) HCl and 10 g CKD (containing CaO = 44.47%) were added to 1000 mL of distilled water (DW). The mixture was stirred at 250 rpm for 30 min at room temperature and then filtered, yielding a Ca^{2+}-containing filtrate and a solid residue (filter cake). The mass of $CaCl_2$ obtained was 8 g, corresponding to an extraction efficiency of 90.90%.

Step two: 20 g of WTS (containing Al_2O_3 = 20.31%) was used for the extraction of Al^{+3} by following the same procedure described in step one. The mass of $AlCl_3$ obtained was 17.67 g, corresponding to an extraction efficiency of 88.35%.

To create the primary liquid for the necessary ions, the clear solutions of Ca^{+2} and Al^{+3} from steps (1) and (2) were combined in a beaker with a molar ratio of 1:1 (5 g of $CaCl_2$ and 6 g of $AlCl_3$) while being vigorously stirred for 15 minutes.

Tween 18 (polysorbate) was added, and 0.5 mL of NaOH (1 M) with a flow rate of 0.1 mL/min was utilized to raise the pH to 8 to form a (Ca/Al)-LDH, and the flasks must be agitated at 700 rpm for 1 h. NaOH addition was stopped once the mixture became gel-like.

After centrifuging the resultant mixture for five minutes at

4000 rpm, it was washed with hot water, centrifuged until the pH reached 7.5, and dried overnight at 50 ℃ in an oven. The same process was used with two different Ca:Al ratios: 0.5:1 and 2:1.

Dissolving 2 g of Na-alginate in 100 mL of distilled water for 24 hours at room temperature while vigorously stirring with a magnetic stirrer. Various amounts of (Ca/Al) nanoparticles were mixed with this solution. Using a 10 mL syringe, dissolve 1.11 g of $CaCl_2$ in 100 mL DW to create 0.1 M of $CaCl_2$ for polymerization and bead production. The beads, which have a diameter of about 4 mm, were stored in 0.0050 M of $CaCl_2$ (0.278 g $CaCl_2$ was prepared by dissolving in 500 mL DW) at 4 ℃ for later use after being cured in this solution for 24 hours. Figure 1 illustrates this process.

The AMX removals (R) are suitable measures to identify the proper parameters for bead manufacture, including the Ca/Al ratio, nanoparticle dosage, and pH of solution.

$$R = \frac{(C_o - C_e)}{C_o} \times 100 \quad (1)$$

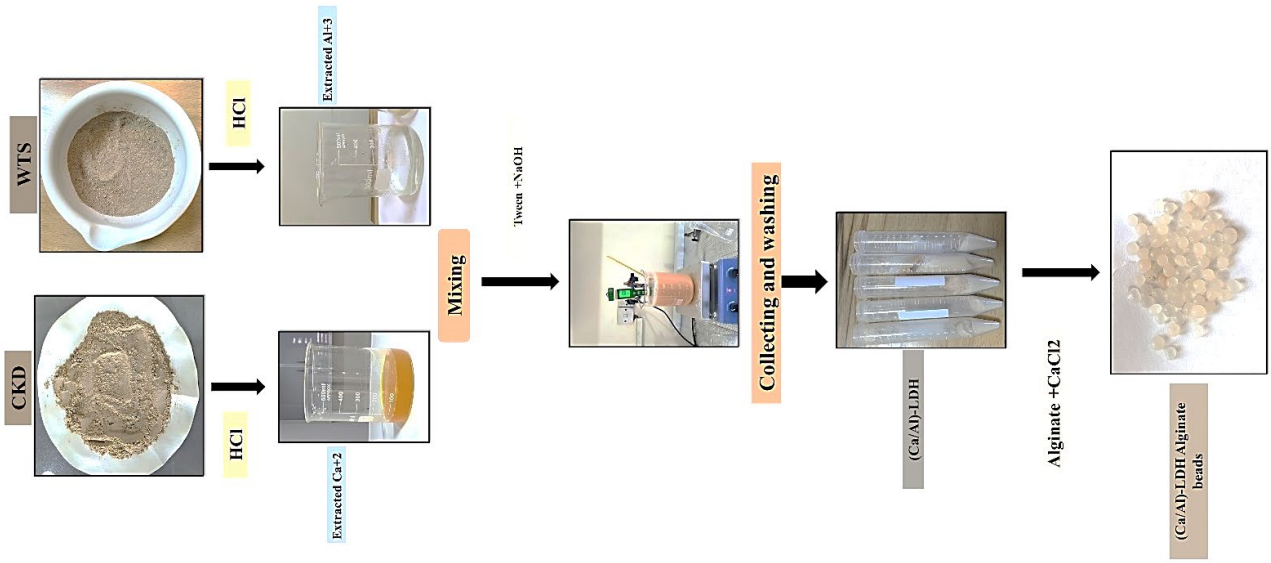

Figure 1. Steps for preparation of Ca/Al nanoparticles and sodium alginate beads

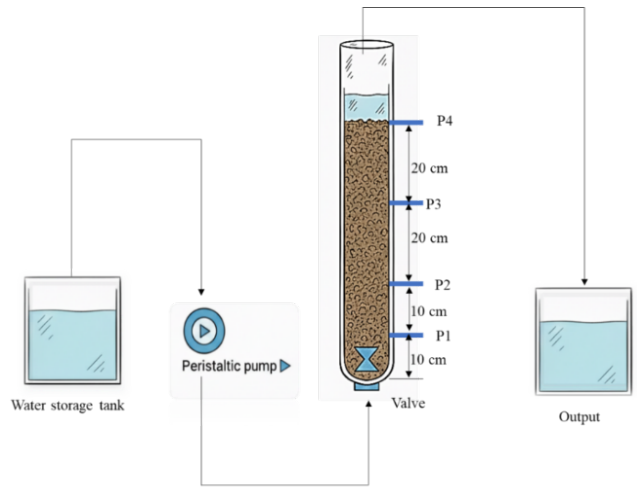

Figure 2. Physical apparatus for monitoring the propagation of amoxicillin (AMX) along the Ca/Al alginate beads

2.3 Column operation mode

A Perspex column, a tank, a valve, a peristaltic pump, and tubes are the main components of the experimental apparatus prepared to study the AMX-water migration. As Figure 2 makes clear, the column's measurements are 2 cm for inner diameter, 70 cm for height, and 3 mm for wall thickness. In order to achieve uniformly moving water, AMX propagation occurs in 1-D through the bed, reflecting the actual conditions in the packed column. The effectiveness of the beads in lowering the concentration of AMX was assessed by filling the column with 60 cm of them. To prevent trapped air, DW must inject in the upward direction. After that, the bed was filled with AMX-contaminated water at intervals of 2, 5, and 10 mL/min until saturation was reached. To guarantee that such a flow is laminar, the groundwater flow characteristics have been established. The columns' ports P1 and P2 are positioned 10 cm from the column entrance, while P3 and P4 are positioned 20 cm. Samples of water have been taken from the ports at exact times in order to determine the AMX contents. The influent's initial AMX concentrations were 10, 50, 100, 150, 200, and 250 mg/L.

2.4 Models for measurements

The C/C_o with elapsed time ("breakthrough curves") can be measured experimentally at selected ports in the packed column, and a set of mathematical models could simulate these curves. PRB may be effectively designed on a field scale using the "breakthrough curve." For a constant, continuous influent concentration, the mentioned curve can be plotted as "S-shaped." The "breakthrough curve" can be used to define the "breakthrough point," a special characteristic. The output concentration that met the water purification goal is represented by this point. For straightforward issues, the equation of solute transport can be solved analytically to plot the breakthrough curves; however, complex circumstances cannot be solved in this way. As a result, computer-assisted semi-analytical solutions and empirical approximations were developed. Applying such tractable and simplified models was

necessary to characterize the AMX migration with a satisfactory level of accuracy as compared to numerical solutions [47]. The empirical and theoretical models used in this investigation are listed in Table 1.

Table 1. Models for the description of experimental outputs

Model	Formula	Reference
Bohart-Adams	$\frac{C}{C_o} = \frac{1}{1 + \exp\left(KNo * \frac{Z}{U} - KC_o t\right)}$	[48]
Yan	$\frac{C}{C_o} = 1 - \frac{1}{1 + (1\left(\left(0.001 \times \frac{C \times Q}{q_o M}\right) \times t\right)^a}$	[49]
Belter-Cussler-Hu	$\frac{C}{C_o} = 1 + \text{erf}(\frac{(t - t_o)\exp\left(-\sigma\left(\frac{t}{t_o}\right)\right)}{\left(\sqrt{2\sigma} t_o\right)})$	[50]
Clark	$\left(\frac{C}{C_o}\right)^{(n-1)} = 1/(1 + A * e^{(-rt)})$	[51]
Thomas-BDST	$\frac{C}{C_0} = \frac{1}{1 + \exp\left[\frac{(Mq_0K_{Th})}{Q} - \frac{K_{Th}C_0t}{1000}\right]}$	[52]

3. RESULTS AND DISCUSSION

3.1 Beads manufacture

The primary objective of the preparation experiments was to specify the bead preparation conditions for the sorption of AMX. The primary production parameters used in this investigation were the Ca:Al ratio, the quantity of nanoparticles, and the water's starting pH. Each condition's ideal value is correlated with a higher AMX elimination. The pH values were 7, 10, and 12 with a Ca/Al ratio of 1:1 and a dosage of 20 g/100 mL of nanoparticles in order to examine the pH effect on the effectiveness of sorbent formation. Tests were effective in identifying the removal process using 2 grams of beads per 50 mL, 100 mg/L of AMX-water, pH 7, and 250 rpm for 3 h. Table 2 illustrates how pH affects the Ca/Al sodium alginate's capacity to eliminate AMX during the manufacturing process. The highest AMX removal effectiveness was recorded at pH 10, with a value of 51%, because the optimal LDH required basic conditions. Changes in acidity may induce a significant decrease in the percentage of removal due to the larger diameter of the nanoparticle. Therefore, pH 10 can be used in the production process. The influence of a Ca to Al ratio between 0.5 and 2 on the formation of beads can be assessed at pH 10. For every 100 milliliters, two grams of (Ca/Al)-LDH nanoparticles were introduced. A molar ratio of 1 was required to achieve the higher removal (43%), according to the results (Table 2). When compared to the maximum level, efficiency can decrease due to either the LDH structural disorder or a change in the radius difference between Ca and Al [48]. The impact of particles grams (5–50 g/100 mL) on sorbent production may be investigated at optimal molar ratio and pH (i.e., 10 & 1, respectively). The significant improvement in AMX removal efficiency is explained by the findings. When the beads are varied from 5 to 50 grams, the effectiveness of AMX elimination may be 45%. The removal of AMX by Ca/Al-LDH–alginate beads is mainly governed by chemisorption, as indicated by the pseudo-second-order kinetic model, and involves electrostatic interactions and surface complexation between the carboxyl groups of AMX and the positively charged Ca^{2+} and Al^{3+} sites on the LDH surface. In addition, the layered structure of LDH allows interlayer anion exchange with AMX species, while hydrogen bonding may contribute as a secondary interaction. These mechanisms have now been briefly explained in the discussion section to provide a clearer interpretation of the adsorption process.

Table 2. Effect of synthesis factors on the removal percentage of amoxicillin (AMX) for tests of sorption at (50 mg/L AMX, beads 0.5 g, 60 min, 25 ℃, pH=7, 250 rpm)

Synthesis Parameter		Removal (%)	Other Parameters
pH	7	43	Ca/Al-LDH = 20 g/100 mL, Ca/Al = 1
	10	51	
	12	51	
Ca/Al	0.5	37	pH = 7, Ca/Al-LDH = 20 g/100 mL
	1	43	
	2	31	
	5	21	
Ca/Al LDH (g/100 mL)	10	39	pH = 7, Ca/Al = 1
	20	44	
	40	45	
	50	45	

3.2 Bead characterization

For CKD and LDH, an XRD test was performed to assess the type of compound generated and its purity. The location and number of the peaks indicate whether the compound is crystalline or amorphous. With peaks at 23, 29.5, 36.5, 39.5, 43.0, and 48.5°, Figure 3 demonstrated that CKD is composed of $CaCO_3$, which is consistent with JCPDS Card No. 05-0586 [40]. In accordance with JCPDS Card No. 37-1496 [39], the anhydrite (calcium sulfate) displayed peaks of low intensity at 25.25, 31.5, 37, 36.5, 41.0, and 45.5°. Quartz and portlandite (calcium hydroxide) were identified as the other secondary compounds, which had peaks at 27.1 and 34.0 degrees. This outcome is in line with the chemical analysis inserted in Table 1. Six peaks at 11.4, 22.9, 31.32, 32.05, 55.2, and 56.8° were identified as belonging to the 002, 004, 110, 112, 030, and 032 crystal planes, respectively, which are the same as the compound made in the study [49].

The size and morphology were measured using SEM and TEM for LDH beads. SEM in Figure 4(a) explained the existence of nano-sheet-like particles with a thickness from 50

to 56 nm in addition to the nano-rod structures with a diameter of 98-100 nm, indicating the formation of the LDH [50]. Compared to the previous studies, the sheet percentage was greater than the rod percentage; this could improve the dispersing agent's effectiveness.

Because the rod's diameter reached 20 nm and the sheet's thickness did not surpass 13 nm, the distinct forms are more visible as distinct particles in TEM analysis. The size is reduced when compared to the SEM result, suggesting that these particles are nano-aggregates in SEM, which were more precisely photographed in TEM (Figure 4(b)). As seen in Figure 4(c), the sorbent shape clearly changes as a result of the attachment of contaminant molecules upon interaction with AMX antibiotic.

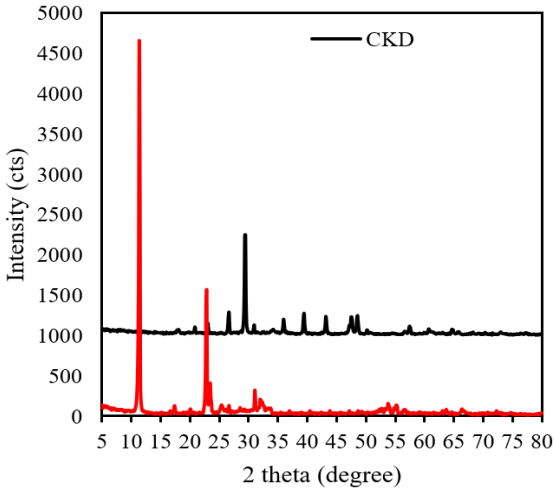

Figure 3. Description of prepared beads and cement kiln dust (CKD) by X-ray Diffraction (XRD)

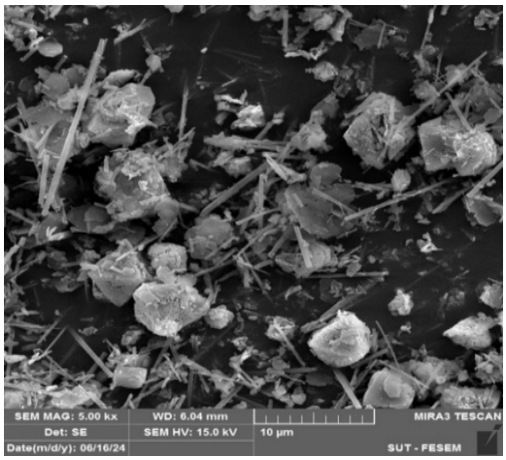

(a) (Ca/Al)-LDH-alginate beads

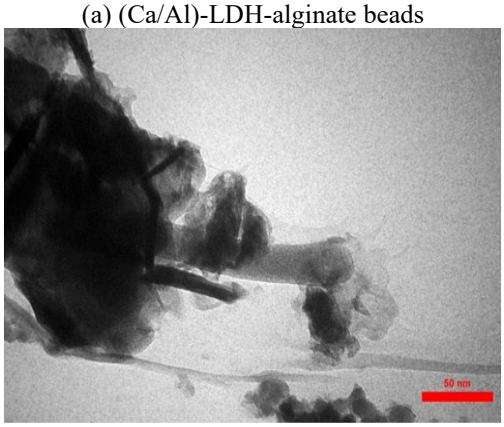

(b) (Ca/Al)-LDH-alginate beads

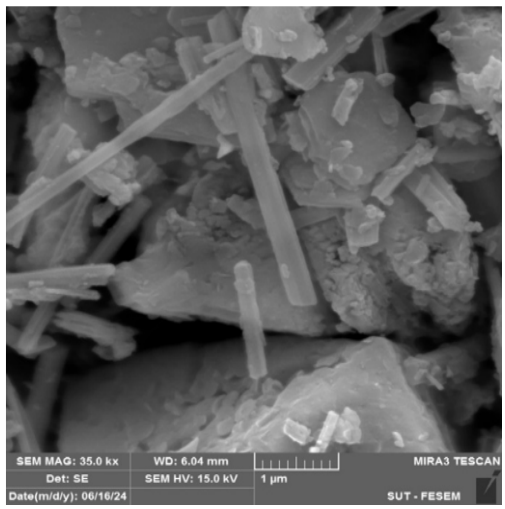

(c) (Ca/Al)-LDH-alginate beads loaded AMX

Figure 4. (a) Scanning Electron Microscopy (SEM) for virgin prepared beads, (b) Transmission Electron Microscopy (TEM) for virgin prepared beads, and (c) SEM for amoxicillin (AMX)-loaded prepared beads

3.3 Continuous outputs

Prepared beads were used as a PRB to evaluate the migration of AMX through a column configuration [51]. Monitoring was done to evaluate how well PRB performed at removing adopted antibiotics from water while keeping permeability within a reasonable range [52]. Conditions used to express (1) the change of AMX C/C_o at P1 and P4 with time and (2) the mathematical formulation of breakthrough curves by Bohart-Adams, Thomas-BDST, Yan, Belter-Cussler-Hu, and Clark models are water flow rate, AMX concentration, and bed depth. The curves in Figures 5 and 6 clearly show the impacts of C_o at 10, 50, 100, 150, 200, and 250 mg/L for 2 mL/min at P1 and P4. These graphs show how, as the influent concentration increases, the beads will be rapidly saturated with AMX. This is because the high concentration gradient increases the driving force for chemical transfer, hastening the depletion of adsorption sites [53].

The breakthrough graphs can be used to determine the "breakthrough time" for the AMX antibiotic that corresponds to 5% C/C_o. The "bed longevity", which is necessary to keep the contaminant in the effluent less than the allowable limit, reflects this time. According to Figure 5, the "breakthrough time" for P1 at a flow rate of 2 mL/min and C_o 10 mg/L is 3.5 days; with C_o 250 mg/L, it is reduced to 0.75 days. This time with C_o for P4 shows a similar pattern; longevity can range from 11.5 to 4 days for C_o 10 and 250 mg/L, respectively, at 2 mL/min. Figures 5 and 6 show the impact of flow rate on the C/C_o front at the same ports for 10, 50, 100, 150, 200, and 250 mg/L. According to these results, the change in flow rate from 2 to 10 mL/min will decrease the "breakthrough time", enhance the appearance of the AMX front, and steepen the "breakthrough curves" because contaminants will leave the beads before they achieve equilibrium [53-56].

Large numbers of adsorbed molecules can also be desorbed from the sorbent's surface by the increased discharge, particularly for weak and reversible bonds. As a result of the increasing effluent concentration, the "breakthrough time" was shortened. For instance, increasing the flow rate from 2 to 10 mL/min for 10 mg/L at P4 can reduce the "breakthrough time" from 11.5 to 7.25 days. As seen in Figures 5 and 6, the higher

sorbent depth considerably delays the development of the AMX front, indicating that the bed depth may affect the contaminant front's spread. The adsorption process is enhanced when AMX molecules have sufficient time to permeate into the deeper pores of the bed. When the thickness of the beads is adjusted from 10 to 60 cm, the "breakthrough time" increases from 3.5 to 11.5 days for 2 mL/min and C_o 10 mg/L; meanwhile, the "saturation duration" increases from 19.5 to 28 days. Because of the increasing surface areas at thicker depths, it is evident that a deeper bed will increase its adsorption capacity for the same C_o [57]. The results demonstrated that the hydraulic conductivity coefficients stay roughly constant at 2.6×10^{-2} cm/s. As a result, during water movement (the migration of contaminants), the pores are still accessible. PRB should have a permeability greater than 2.1×10^{-2} cm/s [54].

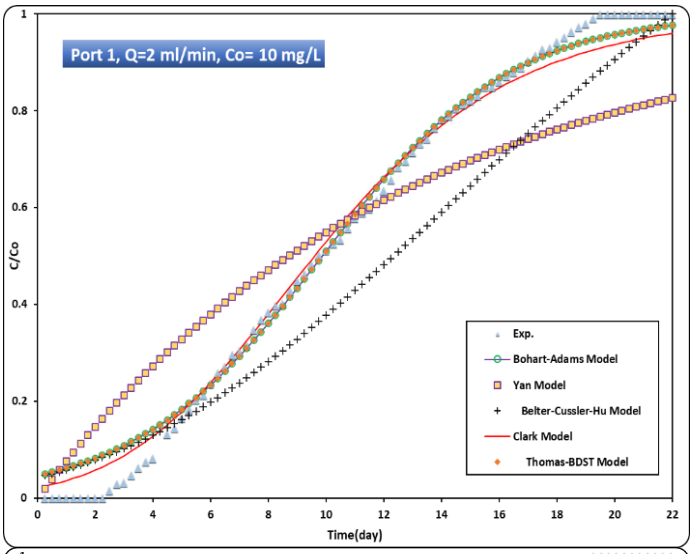

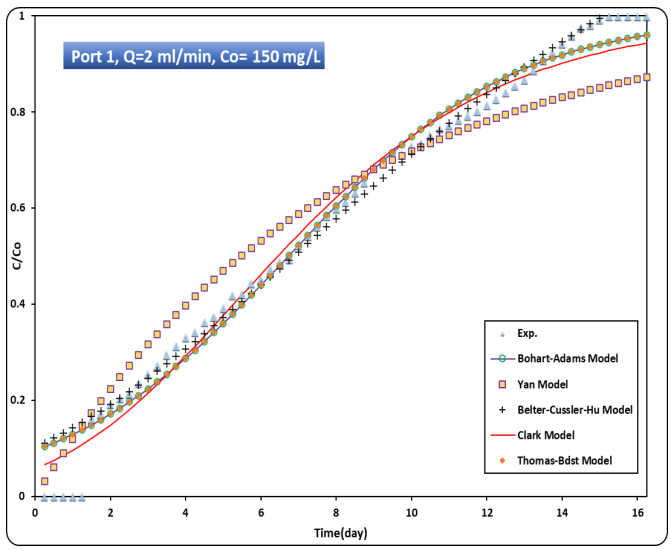

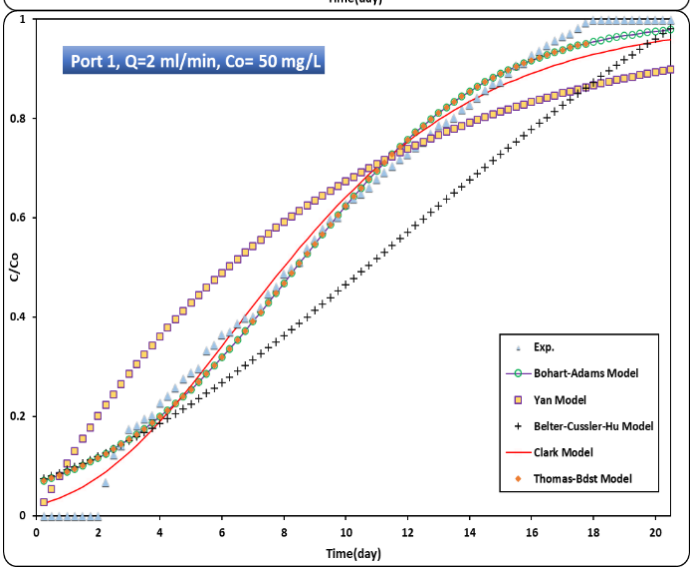

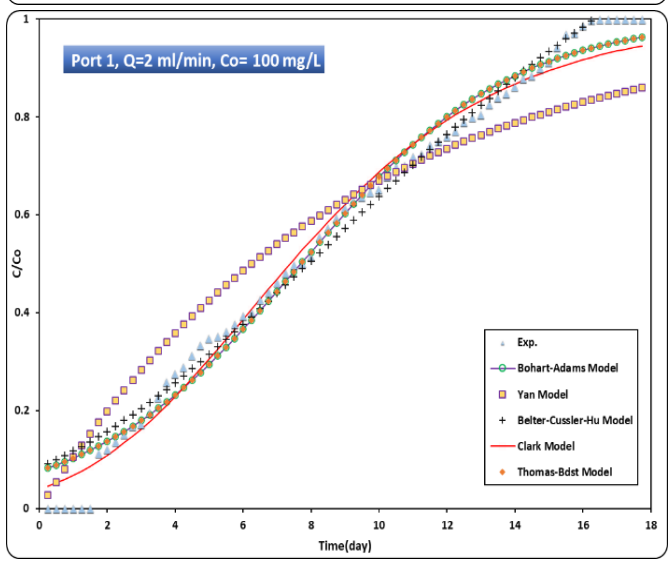

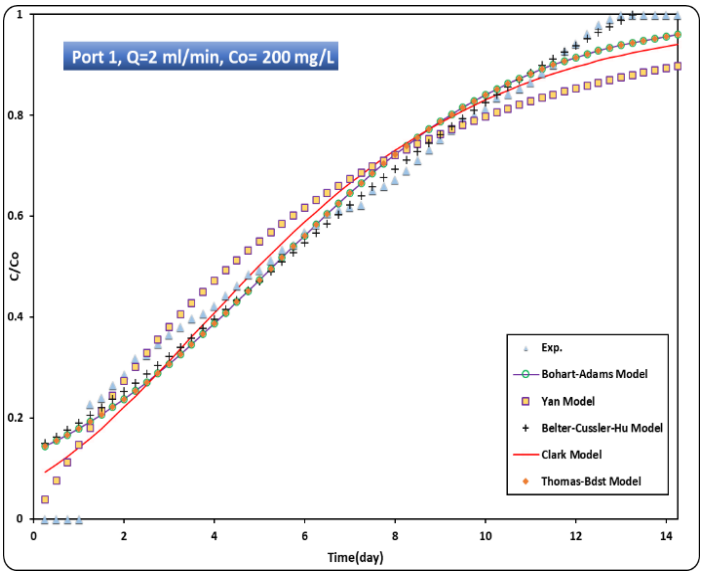

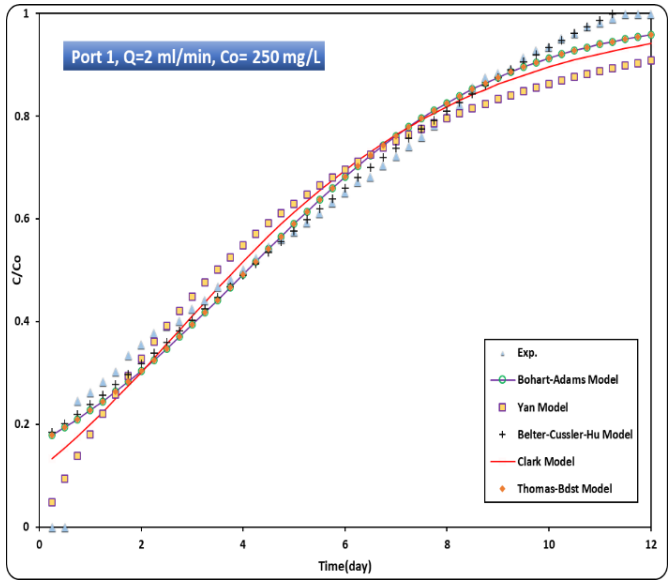

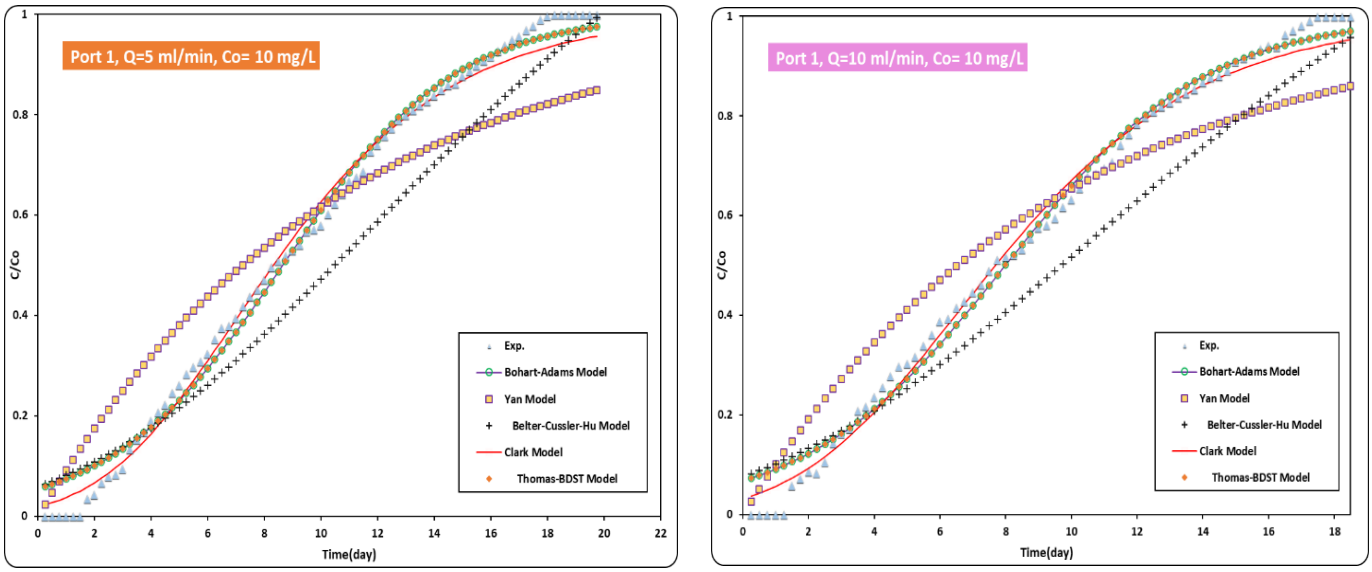

Figure 5. Breakthrough graphs at P1 for the amoxicillin (AMX) propagation

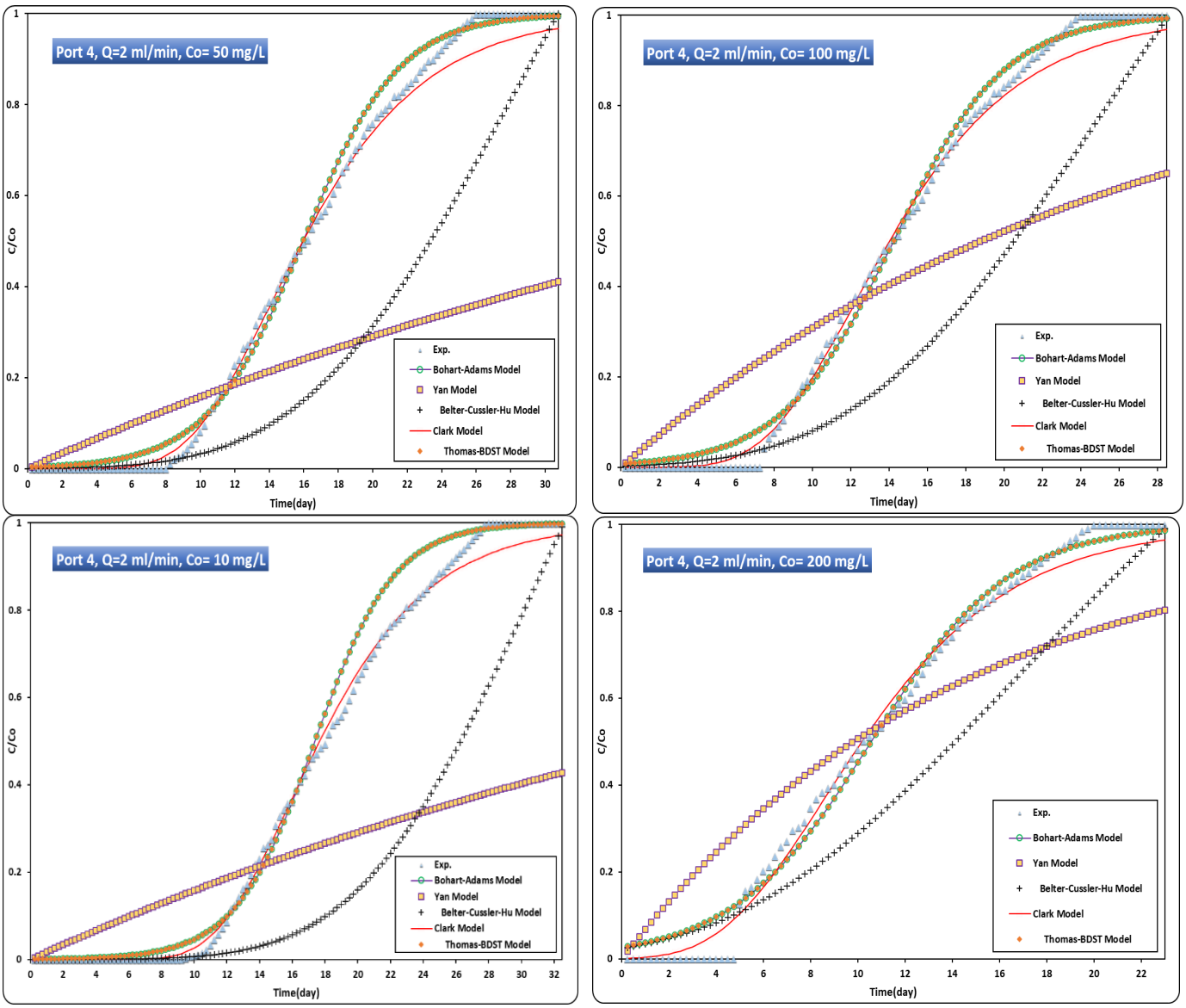

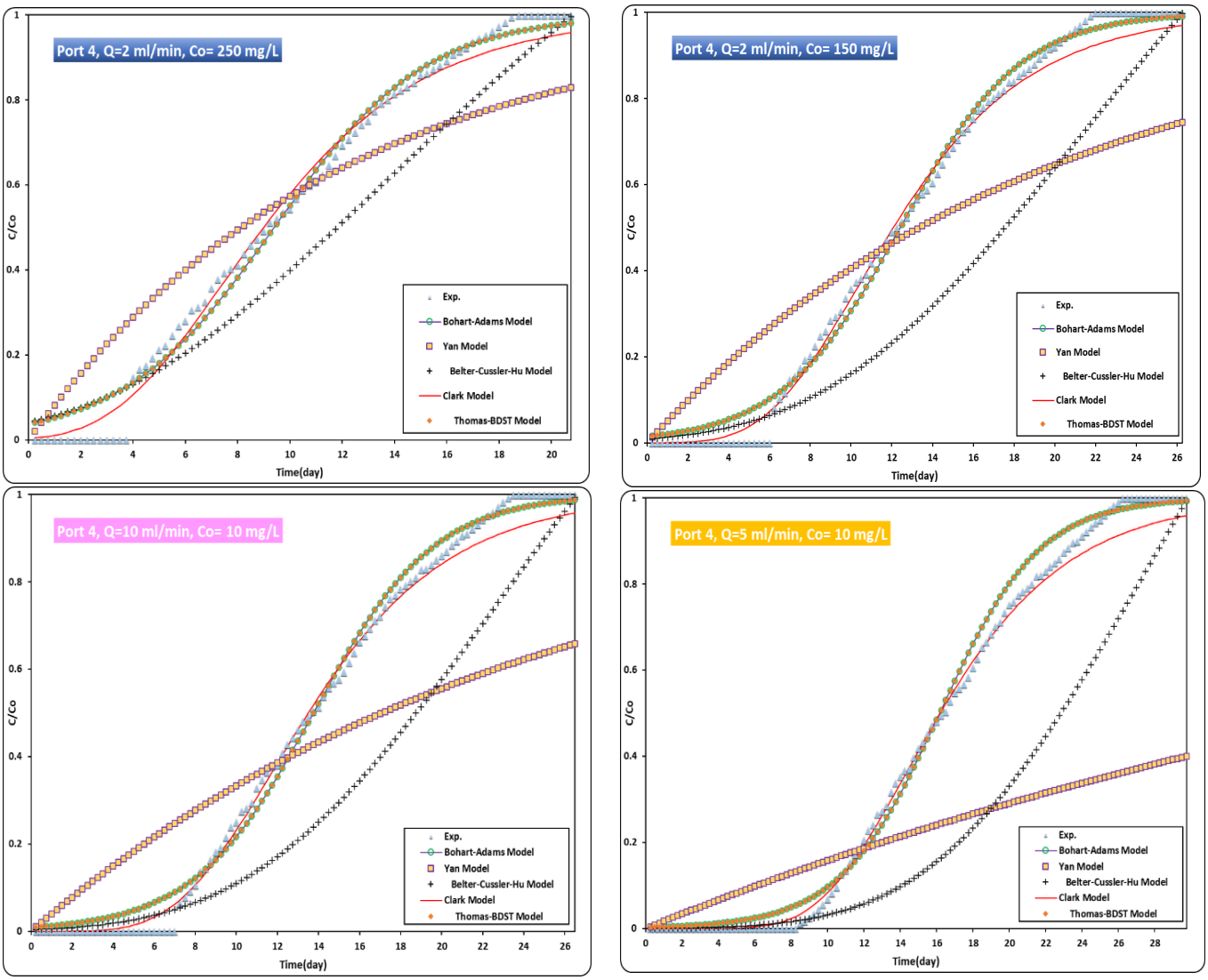

Figure 6. Breakthrough graphs at P4 for the amoxicillin (AMX) propagation

Table 3. Coefficient values for models used to create AMX breakthrough curves at P1 and P4 for various C_o at 2 mL/min

Model	Parameter	P1						P4					
		C_o = 10	**C_o = 50**	**C_o = 100**	**C_o = 150**	**C_o = 200**	**C_o = 250**	**C_o = 10**	**C_o = 50**	**C_o = 100**	**C_o = 150**	**C_o = 200**	**C_o = 250**
Bohart-Adams	KC_o	0.3068	0.3162	0.3225	0.3332	0.3534	0.3973	0.4102	0.3580	0.3432	0.3390	0.3412	0.3438
	KN_o Z/U	3.0286	2.6557	2.4856	2.2426	1.8732	1.6231	7.1333	5.7159	4.886	4.2091	3.6045	3.2324
	R^2	0.9402	0.9882	0.9839	0.9797	0.9622	0.9669	0.9903	0.9949	0.9948	0.9935	0.9900	0.9875
	SSE	0.6614	0.1089	0.1229	0.1254	0.1826	0.1175	0.0336	0.0570	0.0805	0.1042	0.1360	0.1391
Yan	0.001QC/q$_o$M	5.972×10^{-5}	7.7×10^{-5}	4.9×10^{-6}	5.4×10^{-6}	6.2×10^{-6}	7.7×10^{-6}	7.7×10^{-7}	1.39×10^{-7}	1.6×10^{-6}	2.1×10^{-6}	2.3×10^{-6}	7.6×10^{-5}
	a	1332.5	1453.9	22436.1	23359.3	25587.1	25587.1	22300	22300	22300	24339	30720	682.68
	R^2	0.9179	0.9705	0.9752	0.9748	0.9663	0.9586	0.9152	0.9380	0.9384	0.9492	0.9592	0.9664
	SSE	1.3906	0.7335	0.5624	0.3740	0.2392	0.1659	0.8185	1.3931	1.3947	3.504	1.3314	1.1097
Belter-Cussler-Hu	t_0	22.0103	20.968	16.337	15.1095	13.268	11.289	32.620	30.7658	28.6181	26.3045	23.1891	20.8426
	σ	0.4935	0.5507	0.5781	0.6116	0.6716	0.7243	0.2375	0.2872	0.3311	0.3818	0.4429	0.4871
	R^2	0.9135	0.9621	0.9843	0.9822	0.9697	0.9744	0.7780	0.8366	0.8713	0.8980	0.9322	0.9529
	SSE	1.6598	1.0993	0.1164	0.1110	0.1446	0.0888	1.7116	2.3137	2.8442	2.8914	2.0515	1.2350
Clark	A	2.5142	0.1843	1.0175	0.9240	0.01983	0.0250	0.0109	0.01506	0.0387	0.0304	0.0481	0.0582
	r	0.2374	0.2248	0.2485	0.2600	0.2621	0.2990	0.2159	0.2056	0.2110	0.2193	0.2299	0.2366
	n	1.3299	1.0439	1.2168	1.2297	1.0077	1.0114	1.0034	1.0008	1.0028	1.0030	1.0066	1.0099
	R^2	0.9404	0.9907	0.9865	0.9822	0.9657	0.9657	0.9976	0.9982	0.9975	0.9964	0.9939	0.9918
	SSE	0.6457	0.0730	0.1035	0.1113	0.1679	0.1238	0.0072	0.0101	0.0186	0.0326	0.0562	0.0716
Thomas-BDST	KTC_O	0.306	0.3162	0.3225	0.3332	0.3534	0.3973	0.4102	0.3580	0.3432	0.3390	0.3412	0.3438
	KTqM/Q	3.0286	2.6557	2.4856	2.2426	1.8732	1.6231	7.1333	5.7159	4.886	4.2091	3.6045	3.2324
	R^2	0.9402	0.9882	0.9839	0.9797	0.9622	0.9669	0.9903	0.9949	0.9948	0.9935	0.9900	0.9875
	SSE	0.6614	0.1089	0.1229	0.1254	0.1826	0.1175	0.0336	0.0570	0.0805	0.1042	0.1360	0.1391

Table 4. Coefficient values for models used to create AMX breakthrough curves at P1 and P4 for various Q at 50 mg/L

Model	Parameter	P1			P4		
		Q = 2	Q = 5	Q = 10	Q = 2	Q = 5	Q = 10
Bohart-Adams	KC_o	0.3162	0.3162	0.3079	0.3580	0.3406	0.3377
	KN_0 Z/U	2.6557	2.2814	2.0333	5.7159	4.8473	4.1094
	R^2	0.9882	0.9845	0.9804	0.9949	0.9950	0.9926
	SSE	0.1089	0.1079	0.1158	0.0570	0.0706	0.1052
Yan	$0.001QC/q_0M$	7.7×10^{-5}	9.59×10^{-6}	8.78×10^{-6}	1.39×10^{-7}	1.6×10^{-6}	2.2×10^{-6}
	a	1453.9	12384.1	14630.4	22300	22300	24295
	R^2	0.9705	0.9765	0.9743	0.9380	0.9360	0.9459
	SSE	0.7335	0.4185	0.2793	1.3931	1.3599	1.4604
Belter-Cussler-Hu	t_0	20.968	18.2311	17.8331	30.7658	27.5599	24.401
	σ	0.5507	0.6127	0.6488	0.2872	0.3330	0.3903
	R^2	0.9621	0.9790	0.9778	0.8366	0.8957	0.9315
	SSE	1.0993	0.3721	0.3330	2.3137	2.3962	2.0229
Clark	A	0.1843	1.4727	1.2056	0.01506	0.02875	0.0233
	r	0.2248	0.25484	0.2499	0.2056	0.2089	0.2194
	n	1.0439	1.3219	1.3172	1.0008	1.0022	1.0025
	R^2	0.9907	0.9865	0.9824	0.9982	0.9976	0.9959
	SSE	0.0730	0.0953	0.1058	0.0101	0.0132	0.0328
Thomas-BDST	KTC_O	0.3162	0.3162	0.3079	0.3580	0.3406	0.3377
	KTqM/Q	2.6557	2.2814	2.0333	5.7159	4.8473	4.1094
	R^2	0.9882	0.9845	0.9804	0.9949	0.9950	0.9926
	SSE	0.1089	0.1079	0.1158	0.0570	0.0706	0.1052

Experimental data from ongoing column testing for AMX removal were used to fit the aforementioned models at P1 and P4. The models' fitted parameters (Tables 3 and 4) demonstrated that the adsorption capacity for AMX is significantly increased with higher alginate beads [58-64]. Using the Solver Excel spreadsheet tool, nonlinear fitting was used to find the coefficients of the models as inserted in Tables 3 and 4. A suitable model that can be adopted to estimate the "breakthrough point" on the plotted curves was specified by calculating "sum of squared errors, SSE" and "coefficient of determination, R^2". The measurements at P1 and P4 were best represented by the Bohart-Adams, with $R^2 > 0.98$ and SSE < 0.15.

4. CONCLUSIONS

Using a combination of calcium ion solution and aluminum ion solution extracted using the precipitation method, Ca/Al-LDH nanoparticles were successfully created. In order to create a novel sorbent called Ca/Al-LDH—beads—PRB for the treatment of contaminated groundwater, the produced nanoparticles needed to be immobilized by Na-alginate. Because of the utilization of byproducts in the manufacturing of such bead sorbent, this work examined the actual step in the sustainable development. Ca to Al = 1, pH = 10, and particle dosage = 45 g/100 mL are the proper parameters for bead synthesis. The characterization investigations confirmed that nanoparticles had developed within the produced sorbent and might aid in AMX sorption. The results of PRB's ability to prevent AMX migration demonstrate that PRB lifetime can be increased by lowering the inlet concentration, lowering the water flow rate, and increasing the quantity of beads. Therefore, at the lowest flow rate (2 mL/min), concentration (10 mg/L), and higher depth (60 cm), the greatest values for breakthrough time and saturation time were 11.5 and 28 days, respectively. The Bohart-Adams model proved suitable for creating the column test data. In this model, K typically decreases as C_o increases, reflecting that higher C_o leads to faster saturation of adsorption sites and a lower apparent adsorption rate per unit concentration. Similarly, other parameters vary with C_o or q_e to reflect changes in bed capacity, mass transfer, and overall adsorption dynamics. The results demonstrated that the voids in the packed beds are still able to carry water, with a permeability coefficient of 2.6×10^{-2} cm/s.

REFERENCES

[1] Chowdhury, S., Saha, P. (2011). Adsorption kinetic modeling of Safranin onto rice husk biomatrix using pseudo-first- and pseudo-second-order kinetic models: Comparison of linear and non-linear methods. Clean Soil Air Water, 39(3): 274-282. https://doi.org/10.1002/clen.201000170

[2] Chowdhury, S., Balasubramanian, R. (2014). Graphene/semiconductor nanocomposites (GSNs) for heterogeneous photocatalytic decolorization of wastewaters contaminated with synthetic dyes: A review. Applied Catalysis B: Environmental, 160: 307-324. https://doi.org/10.1016/j.apcatb.2014.05.035

[3] Hall, P.L., Quam, H. (1976). Countermeasures to control oil spills in Western Canada. Groundwater, 14(2): 163-169. https://doi.org/10.1111/j.1745-6584.1976.tb00097.x

[4] Naushad, M., Ahamad, T., Sharma, G., Al-Muhtaseb, A.H., Albadarin, A.B., Alam, M.M., AlOthman, Z.A., Alshehri, S.M., Ghfar, A.A. (2016). Synthesis and characterization of a new starch/SnO_2 nanocomposite for efficient adsorption of toxic Hg^{2+} metal ion. Chemical Engineering Journal, 300: 306-316. https://doi.org/10.1016/j.cej.2016.04.084

[5] Tatarchuk, T., Paliychuk, N., Bitra, R.B., Shyichuk, A., Naushad, M., Mironyuk, I., Ziolkowska, D. (2019). Adsorptive removal of toxic Methylene Blue and Acid Orange 7 dyes from aqueous medium using cobalt-zinc ferrite nanoadsorbents. Desalination and Water Treatment, 150: 374-385. https://doi.org/10.5004/dwt.2019.23751

[6] Naushad, M. (2014). Surfactant assisted nano-composite cation exchanger: Development, characterization and applications for the removal of toxic Pb^{2+} from aqueous medium. Chemical Engineering Journal, 235: 100-108. https://doi.org/10.1016/j.cej.2013.09.013

[7] Yousaf, B., Amina, Liu, G., Wang, R., Imtiaz, M., Rizwan, M.S., Zia-ur-Rehman, M., Qadir, A., Si, Y. (2016). The importance of evaluating metal exposure and predicting human health risks in urban-periurban environments influenced by emerging industry. Chemosphere, 150: 79-89. https://doi.org/10.1016/j.chemosphere.2016.02.007

[8] Yousaf, B., Liu, G., Abbas, Q., Wang, R., Ullah, H., Mian, M.M., Amina, Rashid, A. (2018). Enhanced removal of hexavalent chromium from aqueous media using a highly stable and magnetically separable rosin-biochar-coated TiO_2@C nanocomposite. RSC Advances, 8: 25983-25996. https://doi.org/10.1039/C8RA02860E

[9] Blowes, D.W., Puls, R.W., Gillham, R.W., Ptacek, C.J., et al. (1999). An In Situ Permeable Reactive Barrier for the Treatment of Hexavalent Chromium and Trichloroethylene in Ground Water: Volume 2 Performance Monitoring. EPA.

[10] Gillham, R.W., Burris, D.R. (1997). Recent developments in permeable in situ treatment walls for remediation of contaminated groundwater.

[11] Travis, C., Doty, C. (1990). ES&T views: Can contaminated aquifers at superfund sites be remediated? Environmental Science & Technology, 24(10), 1464-1466. https://doi.org/10.1021/es00080a600

[12] Faisal, A.A.H., Sulaymon, A.H., Khaliefa, Q.M. (2018). A review of permeable reactive barrier as passive sustainable technology for groundwater remediation. International Journal of Environmental Science and Technology, 15(5): 1123-1138. https://doi.org/10.1007/s13762-017-1466-0

[13] Faisal, A.A.H., Ali, I.M., Naji, L.A., Madhloom, H.M., Al-Ansari, N. (2020). Using different materials as permeable reactive barrier for remediation of groundwater contaminated with landfill's leachate. Desalination and Water Treatment, 175: 152-163. https://doi.org/10.5004/dwt.2020.24890

[14] Faisal, A.A.H., Hmood, Z.A. (2015). Groundwater protection from cadmium contamination by zeolite permeable reactive barrier. Desalination and Water Treatment, 53(5), 1377-1386. https://doi.org/10.1080/19443994.2013.855668

[15] Faisal, A.A.H., Abbas, T.R., Jassam, S.H. (2015). Removal of zinc from contaminated groundwater by zero-valent iron permeable reactive barrier. Desalination and Water Treatment, 55(6): 1586-1597. https://doi.org/10.1080/19443994.2014.928908

[16] Faisal, A.A.H. (2016). Effect of pH on the performance of olive pips reactive barrier through the migration of copper-contaminated groundwater. Desalination and Water Treatment, 57(11): 4935-4943. https://doi.org/10.1080/19443994.2014.999132

[17] Sulaymon, A.H., Faisal, A.A.H., Khaliefa, Q.M. (2015). Cement kiln dust (CKD)-filter sand permeable reactive barrier for the removal of Cu(II) and Zn(II) from simulated acidic groundwater. Journal of Hazardous Materials, 297: 160-172. https://doi.org/10.1016/j.jhazmat.2015.04.061

[18] Faisal, A.A.H., Al-Wakel, S.F.A., Assi, H.A., Naji, L.A., Naushad, M. (2020). Waterworks sludge-filter sand permeable reactive barrier for removal of toxic lead ions from contaminated groundwater. Journal of Water Process Engineering, 33: 101112. https://doi.org/10.1016/j.jwpe.2019.101112

[19] Faisal, A.A.H., Ahmed, M.D. (2015). Removal of copper ions from contaminated groundwater using waste foundry sand as permeable reactive barrier. International Journal of Environmental Science and Technology, 12(8): 2613-2622. https://doi.org/10.1007/s13762-014-0670-4

[20] Naji, L.A., Faisal, A.A.H., Rashid, H.M., Naushad, M., Ahamad, T. (2020). Environmental remediation of synthetic leachate produced from sanitary landfills using low-cost composite sorbent. Environmental Technology & Innovation, 18: 100680. https://doi.org/10.1016/j.eti.2020.100680

[21] Faisal, A.A., Abd, Z.T.A. (2015). Using granular dead anaerobic sludge as permeable reactive barrier for remediation of groundwater contaminated with phenol. Journal of Environmental Engineering, 141(4): 04014072. https://doi.org/10.1061/(ASCE)EE.1943-7870.0000903

[22] Faisal, A.A., Abd Ali, Z.T. (2017). Using sewage sludge as a permeable reactive barrier for remediation of groundwater contaminated with lead and phenol. Separation Science and Technology, 52(4): 732-742. https://doi.org/10.1080/01496395.2016.1251463

[23] Rashid, M.H., Faisal, A.A. (2018). Removal of dissolved cadmium ions from contaminated wastewater using raw scrap zero-valent iron and zero-valent aluminum as locally available and inexpensive sorbent wastes. Iraqi Journal of Chemical and Petroleum Engineering, 19(4): 39-45. https://doi.org/10.31699/ijcpe.2018.4.5

[24] Rashid, H.M., Faisal, A.A. (2019). Removal of dissolved trivalent chromium ions from contaminated wastewater using locally available raw scrap iron-aluminum waste. Al-Khwarizmi Engineering Journal, 15(1): 134-143. https://doi.org/10.22153/kej.2019.03.006

[25] Alquzweeni, S.S., Faisal, A.A. (2020). Possibility of using granular iron slag byproduct as permeable reactive barrier for remediation of simulated water contaminated with lead ions. Desalination and Water Treatment, 178: 211-219. https://doi.org/10.5004/dwt.2020.24974

[26] Faisal, A.A.H., Alquzweeni, S.S., Naji, L.A., Naushad, M. (2020). Predominant mechanisms in the treatment of wastewater due to interaction of benzaldehyde and iron slag byproduct. International Journal of Environmental Research and Public Health, 17(1): 226. https://doi.org/10.3390/ijerph17010226

[27] Balasubramani, K., Sivarajasekar, N., Naushad, M. (2020). Effective adsorption of antidiabetic pharmaceutical (metformin) from aqueous medium using graphene oxide nanoparticles: Equilibrium and statistical modelling. Journal of Molecular Liquids, 301: 112426. https://doi.org/10.1016/j.molliq.2019.112426

[28] Sharma, G., Naushad, M. (2020). Adsorptive removal of noxious cadmium ions from aqueous medium using activated carbon/zirconium oxide composite: Isotherm and kinetic modelling. Journal of Molecular Liquids, 310: 113025. https://doi.org/10.1016/j.molliq.2020.113025

[29] Sharma, G., Thakur, B., Kumar, A., Sharma, S., Naushad, M., Stadler, F.J. (2020). Gum acacia-cl-

poly(acrylamide)@carbon nitride nanocomposite hydrogel for adsorption of ciprofloxacin and its sustained release in artificial ocular solution. Macromolecular Materials and Engineering, 305(9): 2000274. https://doi.org/10.1002/mame.202000274

[30] Sharma, G., Thakur, B., Kumar, A., Sharma, S., Naushad, M., Stadler, F.J. (2020). Atrazine removal using chitin-cl-poly(acrylamide-co-itaconic acid) nanohydrogel: Isotherms and pH responsive nature. Carbohydrate Polymers, 241: 116258. https://doi.org/10.1016/j.carbpol.2020.116258

[31] Faisal, A.A., Abdul-Kareem, M.B., Mohammed, A.K., Naushad, M., Ghfar, A.A., Ahamad, T. (2020). Humic acid coated sand as a novel sorbent in permeable reactive barrier for environmental remediation of groundwater polluted with copper and cadmium ions. Journal of Water Process Engineering, 36: 101373. https://doi.org/10.1016/j.jwpe.2020.101373

[32] Tas, A.C. (2000). Synthesis of biomimetic Ca-hydroxyapatite powders at 37 °C in synthetic body fluids. Biomaterials, 21(14): 1429-1438. https://doi.org/10.1016/S0142-9612(00)00019-3

[33] Sandrine, B., Ange, N., Didier, B.-A., Eric, C., Patrick, S. (2007). Removal of aqueous lead ions by hydroxyapatites: Equilibria and kinetic processes. Journal of Hazardous Materials, 139(3): 443-446. https://doi.org/10.1016/j.jhazmat.2006.02.039

[34] Davydova, S. (2005). Heavy metals as toxicants in big cities. Microchemical Journal, 79(1-2): 133-136. https://doi.org/10.1016/j.microc.2004.06.010

[35] Basibuyuk, M., Kalat, D.G. (2004). The use of waterworks sludge for the treatment of vegetable oil refinery industry wastewater. Environmental Technology, 25(3): 373-380. https://doi.org/10.1080/09593330409355471

[36] Al-Sajad, M.S., Alsalim, H.A.A. (2024). Evaluation of biosurfactant producing and antimicrobial resistance Pseudomonas for heavy metals tolerance. Iraqi Journal of Agricultural Sciences, 55(Special Issue): 52-62. https://doi.org/10.36103/ijas.v55iSpecial.1885

[37] Hala, M.A., Haider, N.H. (2024). The antibacterial activity of glycolipopeptide produced from Lactococcus lactis HN21 against some clinical pathogens in combination with standard antibiotics. Iraqi Journal of Agricultural Sciences, 55(Special Issue): 12-24. https://doi.org/10.36103/ijas.v55iSpecial.1881

[38] Alshehri, S.M., Naushad, M., Ahamad, T., Alothman, Z.A., Aldalbahi, A. (2014). Synthesis, characterization of curcumin based ecofriendly antimicrobial bio-adsorbent for the removal of phenol from aqueous medium. Chemical Engineering Journal, 254: 181-189. https://doi.org/10.1016/j.cej.2014.05.100

[39] Liu, Y., Chen, S., Chen, X., Zhang, J., Gao, B. (2015). Interactions between Microcystis aeruginosa and coexisting amoxicillin contaminant at different phosphorus levels. Journal of Hazardous Materials, 297: 83-91. https://doi.org/10.1016/j.jhazmat.2015.04.064

[40] Cheung, W.H., Szeto, Y.S., McKay, G. (2007). Intraparticle diffusion processes during acid dye adsorption onto chitosan. Bioresource Technology, 98(15): 2897-2904. https://doi.org/10.1016/j.biortech.2006.09.045

[41] Li, H., Hu, J., Wang, C., Wang, X. (2017). Removal of amoxicillin in aqueous solution by a novel chicken feather carbon: Kinetic and equilibrium studies. Water, Air, & Soil Pollution, 228(6): 201. https://doi.org/10.1007/s11270-017-3385-6

[42] Zhou, Y., Zhang, L., Cheng, Z. (2015). Removal of organic pollutants from aqueous solution using agricultural wastes: A review. Journal of Molecular Liquids, 212: 739-762. https://doi.org/10.1016/j.molliq.2015.10.023

[43] Eniola, J.O., Kumar, R., Mohamed, O.A., Al-Rashdi, A.A., Barakat, M.A. (2020). Synthesis and characterization of CuFe2O4/NiMgAl-LDH composite for the efficient removal of oxytetracycline antibiotic. Journal of Saudi Chemical Society, 24(1): 139-150. https://doi.org/10.1016/j.jscs.2019.11.001

[44] Faisal, A.A.H., Shihab, A.H., Naushad, M., Ahamad, T., Sharma, G., Al-Sheetan, K.M. (2021). Green synthesis for novel sorbent of sand coated with (Ca/Al)-layered double hydroxide for the removal of toxic dye from aqueous environment. Journal of Environmental Chemical Engineering, 9(4): 105342. https://doi.org/10.1016/j.jece.2021.105342

[45] Wang, Y., Gong, S., Li, Y., Li, Z., Fu, J. (2020). Adsorptive removal of tetracycline by sustainable ceramsite substrate from bentonite/red mud/pine sawdust. Scientific Reports, 10(1): 2960. https://doi.org/10.1038/s41598-020-59850-2

[46] Colangelo, F., Cioffi, R. (2013). Use of cement kiln dust, blast furnace slag and marble sludge in the manufacture of sustainable artificial aggregates by means of cold bonding pelletization. Materials, 6(8): 3139-3159. https://doi.org/10.3390/ma6083139

[47] Chu, K.H. (2004). Improved fixed bed models for metal biosorption. Chemical Engineering Journal, 97(2-3): 233-239. https://doi.org/10.1016/S1385-8947(03)00214-6

[48] Milagres, J.L., Bellato, C.R., Vieira, R.S., Ferreira, S.O., Reis, C. (2017). Preparation and evaluation of the Ca-Al layered double hydroxide for removal of copper(II), nickel(II), zinc(II), chromium(VI) and phosphate from aqueous solutions. Journal of Environmental Chemical Engineering, 5(6): 5469-5480. https://doi.org/10.1016/j.jece.2017.10.013

[49] Kim, T.H., Kim, H.J., Oh, J.M. (2012). Interlayer structure of bioactive molecule, 2-aminoethanesulfonate, intercalated into calcium-containing layered double hydroxides. Journal of Nanomaterials, 2012(1): 987938. https://doi.org/10.1155/2012/987938

[50] Ahmed, Z.A., Faisal, A.A. (2023). Precipitation of calcium-aluminum-cetyltrimethylammonium bromide nanoparticles on sand to generate novel adsorbent for elimination of amoxicillin from aquatic environment. Alexandria Engineering Journal, 66: 489-503. https://doi.org/10.1016/j.aej.2022.11.019

[51] Andreozzi, R., Caprio, V., Ciniglia, C., de Champdoré, M., et al. (2004). Antibiotics in the environment: Occurrence in Italian STPs, fate, and preliminary assessment on algal toxicity of amoxicillin. Environmental Science & Technology, 38(24): 6832-6838. https://doi.org/10.1021/es049509a

[52] Liao, P., Zhan, Z., Dai, J., Wu, X., Zhang, W., Wang, K., Yuan, S. (2013). Adsorption of tetracycline and chloramphenicol in aqueous solutions by bamboo charcoal: A batch and fixed-bed column study. Chemical Engineering Journal, 228: 496-505.

https://doi.org/10.1016/j.cej.2013.04.118
[53] Gurumoorthy, N., Arunachalam, K. (2016). Micro and mechanical behaviour of treated used foundry sand concrete. Construction and Building Materials, 123: 184-190. https://doi.org/10.1016/j.conbuildmat.2016.06.143
[54] Faisal, A.A.H., Ahmed, D.N., Rezakazemi, M., Sivarajasekar, N., Sharma, G. (2021). Cost-effective composite prepared from sewage sludge waste and cement kiln dust as permeable reactive barrier to remediate simulated groundwater polluted with tetracycline. Journal of Environmental Chemical Engineering, 9(3): 105194. https://doi.org/10.1016/j.jece.2021.105194
[55] Arica, M.Y., Kaçar, Y., Genç, Ö. (2001). Entrapment of white-rot fungus Trametes versicolor in Ca-alginate beads: Preparation and biosorption kinetic analysis for cadmium removal from an aqueous solution. Bioresource Technology, 80(2): 121-129. https://doi.org/10.1016/s0960-8524(01)00084-0
[56] Ko, D.C.K., Porter, J.F., McKay, G. (2000). Optimised correlations for the fixed-bed adsorption of metal ions on bone char. Chemical Engineering Science, 55(23): 5819-5829. https://doi.org/10.1016/S0009-2509(00)00416-4
[57] Bear, J., Cheng, A.H.D. (2010). Modeling Groundwater Flow and Contaminant Transport. Dordrecht: Springer. https://doi.org/10.1007/978-1-4020-6682-5
[58] Arias, F., Sen, T.K. (2009). Removal of zinc metal ion (Zn^{2+}) from its aqueous solution by kaolin clay minerals: A kinetic and equilibrium study. Colloids and Surfaces A: Physicochemical and Engineering Aspects, 348(1-3): 100-108. https://doi.org/10.1016/j.colsurfa.2009.06.036
[59] Ataklti, A., Alemu, K., Abebe, B. (2016). Study of the self-association of amoxicillin, thiamine and the hetero-association with biologically active compound chlorogenic acid. African Journal of Pharmacy and Pharmacology, 10(18): 393-402. https://doi.org/10.5897/AJPP2016.4542
[60] Revellame, E.D., Fortela, D.L., Sharp, W., Hernandez, R., Zappi, M.E. (2020). Adsorption kinetic modeling using pseudo-first order and pseudo-second order rate laws: A review. Cleaner Engineering and Technology, 1: 100032. https://doi.org/10.1016/j.clet.2020.100032
[61] Elmolla, E.S., Chaudhuri, M. (2010). Photocatalytic degradation of amoxicillin, ampicillin and cloxacillin antibiotics in aqueous solution using UV/TiO2 and UV/H2O2/TiO2 photocatalysis. Desalination, 252(1-3): 46-52. https://doi.org/10.1016/j.desal.2009.11.003
[62] Faisal, A.A.H., Naji, L.A. (2019). Simulation of ammonia nitrogen removal from simulated wastewater by sorption onto waste foundry sand using artificial neural network. Association of Arab Universities Journal of Engineering Sciences, 26(1): 28-34. https://doi.org/10.33261/jaaru.2019.26.1.004
[63] Ho, Y.S. (2006). Review of second-order models for adsorption systems. Journal of Hazardous Materials B, 136(3): 681-689. https://doi.org/10.1016/j.jhazmat.2005.12.04
[64] Bujdák, J. (2020). Adsorption kinetics models in clay systems. The critical analysis of pseudo-second order mechanism. Applied Clay Science, 191: 105630. https://doi.org/10.1016/j.clay.2020.105630

NOMENCLATURE

Latin symbols (Dimensional)

A	Empirical constant in Clark model, dimensionless
C	Concentration of amoxicillin at time t, mg/L
C_0	Initial concentration of amoxicillin (influent concentration), mg/L
C_e	Equilibrium concentration of amoxicillin, mg/L
C_o	Outlet/effluent concentration of amoxicillin, mg/L
D	Diameter of column, cm
DW	Distilled water
H	Height of column, cm
K	Adsorption rate constant, various units depending on model
K_C	Adsorption rate constant with respect to concentration in Bohart-Adams model, L/(mg·min)
KN_o	Adsorption rate constant in Bohart-Adams model, L/(mg·min)
K_{Th}	Adsorption rate constant in Thomas-BDST model, mL/(µg·min)
M	Mass of adsorbent (beads) in column, g
n	Empirical constant in Clark model, dimensionless
Q	Volumetric flow rate, mL/min
R	Removal efficiency or removal percentage, %
r	Reaction rate constant in Clark model, min^{-1}
t	Time, min
t_0	Characteristic time in Belter-Cussler-Hu model, min
U	Superficial velocity or flow velocity, cm/min
Z	Bed depth or column height, cm
a	Empirical constant in Yan model, dimensionless
q_0	Maximum adsorption capacity of adsorbent, mg/g

Greek symbols

σ	Dispersion parameter in Belter-Cussler-Hu model, dimensionless

Dimensionless groups and ratios

C/C_0	Normalized concentration or breakthrough ratio, dimensionless
Ca/Al	Molar ratio of calcium to aluminum in layered double hydroxide, dimensionless
Erf	Error function, dimensionless
Exp	Exponential function, dimensionless

Subscripts and superscripts

0 or o	Initial or inlet condition
E	Equilibrium condition
C	Related to concentration
No	Related to the Bohart-Adams model parameter
Th	Related to the Thomas-BDST model parameter
+2	Divalent cation charge (e.g., Ca^{+2}, Al^{+3})
+3	Trivalent cation charge

Abbreviations and acronyms

AMX	Amoxicillin ($C_{16}H_{19}N_3O_5S$)
Ca-HAP	Calcium hydroxyapatite ($Ca_{10}(PO_4)_6(OH)_2$)
CKD	Cement kiln dust
DW	Distilled water
HAP	Hydroxyapatite
HCl	Hydrochloric acid
LDH	Layered double hydroxide
Na-alginate	Sodium alginate
NaOH	Sodium hydroxide
P&T	Pump-and-treat technology
PRB	Permeable reactive barrier
Rpm	Revolutions per minute
SEM	Scanning electron microscopy
TEM	Transmission electron microscopy
WTS	Waterworks sludge
XRD	X-ray diffraction